Electrochromic Devices

Deutsche Ausgabe: DOI: 10.1002/ange.201508112
Internationale Ausgabe: DOI: 10.1002/anie.201508112

Real-time Observation of Deep Lithiation of Tungsten Oxide Nanowires by In Situ Electron Microscopy

Kuo Qi, Jiake Wei, Muhua Sun, Qianming Huang, Xiaomin Li, Zhi Xu, Wenlong Wang, and Xuedong Bai**

Abstract: *An in-depth mechanistic understanding of the electrochemical lithiation process of tungsten oxide (WO_3) is both of fundamental interest and relevant for potential applications. One of the most important features of WO_3 lithiation is the formation of the chemically flexible, non-stoichiometric Li_xWO_3, known as tungsten bronze. Herein, we achieved the real-time observation of the deep electrochemical lithiation process of single-crystal WO_3 nanowires by constructing in situ transmission electron microscopy (TEM) electrochemical cells. As revealed by nanoscale imaging, diffraction, and spectroscopy, it is shown that the rapid and deep lithiation of WO_3 nanowires leads to the formation of highly disordered and near-amorphous Li_xWO_3 phases, but with no detectable traces of elemental W and segregated Li_2O phase formation. These results highlight the remarkable chemical and structural flexibility of the Li_xWO_3 phases in accommodating the rapid and deep lithiation reaction.*

Tungsten oxide (WO_3) is a versatile transition metal oxide functional material that offers unique opportunities for a wide range of applications. Primary interest in studies of the electrochemical lithiation process of WO3 stems from its practical relevance to the WO3-based electrochromic devices that have attracted intense research spanning for several decades due to their significance in energy efficiency technologies such as electrochromic smart windows.[1–6] The lithiation process of WO_3, accounting for electrochromism, can be referred to the following simple reaction:[7,8]

$$x\,Li^+ + x\,e^- + WO_3 \rightarrow Li_xWO_3 \qquad (1)$$

The chemical and structural flexibility of the nonstoichiometric Li_xWO_3 compound, also known as lithium tungsten bronze, constitutes the basis for the working stability of electrochromic devices. Furthermore, this lithiation process also suggests WO_3 can be exploited as a good candidate for the fabrication of high-capacity lithium ion batteries.[9,10]

[*] K. Qi, J. Wei, M. Sun, Q. Huang, X. Li, Z. Xu, Dr. W. Wang, Dr. X. Bai
Beijing National Laboratory for Condensed Matter Physics and Institute of Physics, Chinese Academy of Sciences
Beijing 100190 (China)
E-mail: wwl@iphy.ac.cn
xdbai@iphy.ac.cn
Dr. X. Bai
Collaborative Innovation Center of Quantum Matter
Beijing (China)

Supporting information for this article is available on the WWW under http://dx.doi.org/10.1002/anie.201508112.

Despite the fundamental importance of electrochemical lithiation of WO_3, little is actually known about its microscopic mechanism in terms of the lithium transport and intercalation process, the real-time phase transition, morphological evolution, or the overall electrochemical dynamics. In general, these features have been difficult to measure when testing bulk electrochemical devices. Herein, by taking advantage of in situ transmission electron microscopy (TEM),[11–15] we report the deep electrochemical lithiation process of single-crystalline WO_3 nanowires by nanoscale imaging, diffraction, and spectroscopy. The rapid and deep lithiation of individual WO_3 nanowires was enabled by driving an in situ solid-state electrochemical cell through a Li_2O solid electrolyte layer (Figure 1). More experimental details can be found in the Methods section (Supporting Information).

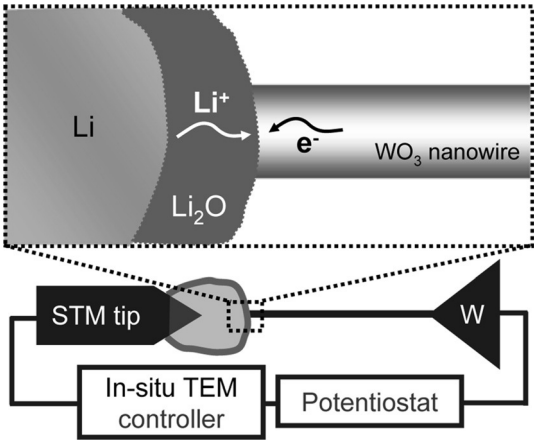

Figure 1. Schematic of the in situ electrochemical cell for the lithiation of WO_3. Li_2O plays the role of the solid electrolyte and the lithium ions arrive at the interface between the WO_3 and Li_2O under the external applied electric field.

When an external constant voltage of −2 V is applied, the contrast of the partial WO_3 nanowire in BF-TEM images changes in the contact zone between the Li_2O thin layer and the pristine WO_3. The interface of the lithiation front emerges in the body of the WO_3 nanowire, which is approximately 180 nm away from the Li_2O-WO_3 contact zone (Figure 2a,b). Figure 2(c,d) show the SAED patterns of the pristine WO_3 and its lithiation front interface, respectively. The enlarged TEM image of the lithiated area and the corresponding SAED result are presented in Figure 2e,f). The intensity of the SAED patterns decreases and the dispersed diffraction halos come into view from Figure 2c to Figure 2d, which

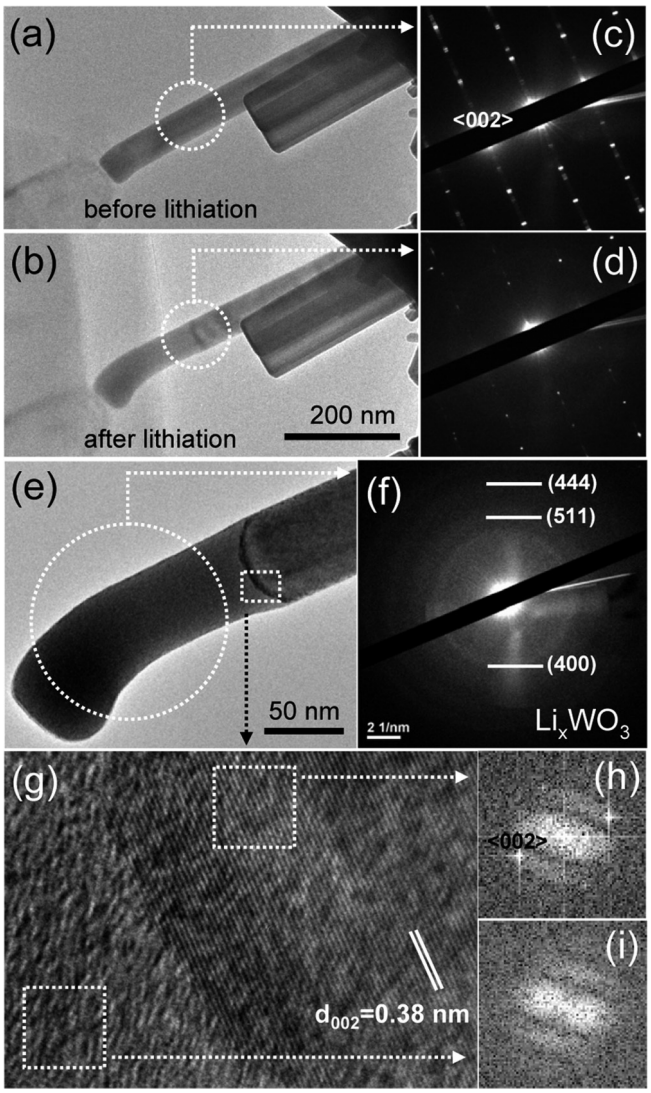

Figure 2. Detailed structural characterization of the final state of the deep lithiation for a single WO_3 nanowire. a, c) Bright-field TEM (BF-TEM) image and selected area electron diffraction (SAED) pattern of the pristine WO_3 nanowire. b, d) The BF-TEM image and SAED pattern of the partly deep lithiated WO_3 nanowire. e) The enlarged TEM image of the deep lithiated area and the lithiation interface. f) The SAED pattern of the deep lithiated section, marked by a dotted circle. g) The high-resolution TEM (HRTEM) image of the lithiation front, representing the area, marked by the dotted rectangle in Figure 2e. h, i) The fast Fourier transform (FFT) patterns of both sides of the lithiation front.

demonstrates that the pristine crystalline structure has been destroyed. The expansion of volume and varied morphology in the lithiation area of the nanowire can be seen clearly from Figure 2(e), reflecting the structural change of the pristine monoclinic phase in the WO_3 nanowire after lithiation. The diffraction rings of the lithiated area (Figure 2f) can be indexed as the cubic Li_xWO_3 phase (JCPDS card No: 47-0500), where x is 0.3. The obvious halos correspond to the (400), (511), and (444) planes of $Li_{0.3}WO_3$.

An arc-shaped contrast can be distinguished clearly (white dotted rectangle, Figure 2e), which represents the lithiation reaction front interface of the single WO_3 nanowire. The detailed structure of the lithiation reaction front is investigated by HRTEM imaging and FFT analysis (Figure 2g–i), respectively. Figure 2(g) is a high-resolution image of the region marked by the white dotted rectangle in Figure 2(e), and reveals the explicit interface between the lithiated and the unlithiated areas. The phase of the lithiated area is amorphous because there is no crystal lattice fringe in the HRTEM image (Figure 2g), and no bright spot is seen in the related FFT pattern (Figure 2i). On the other hand, the unlithiated region has maintained the pristine monoclinic single crystalline phase of WO_3, as clearly evidenced by the interplanar spacing (0.38 nm) of the crystal lattice fringes (Figure 2g), in combination with the two bright spots in the corresponding FFT (Figure 2h). Furthermore, the arc-shaped interface is symmetrical to the central axis of the nanowire, illustrating that the orientation of the lithiation reaction is along the long-axis of the nanowire while the velocity of the lithiation is different between the superficial region and the internal area of the nanowire.

To confirm the structure of the product in the lithiated region, electron energy loss spectroscopy (EELS) was conducted before and after the lithiation of another single WO_3 nanowire. Figure 3a expresses the O K edge EELS and number of fine structures labeled A, D, F, G, and H. The peaks A to H are at 530.6, 537.5, 544.1, 553.3, and 570.1 eV,

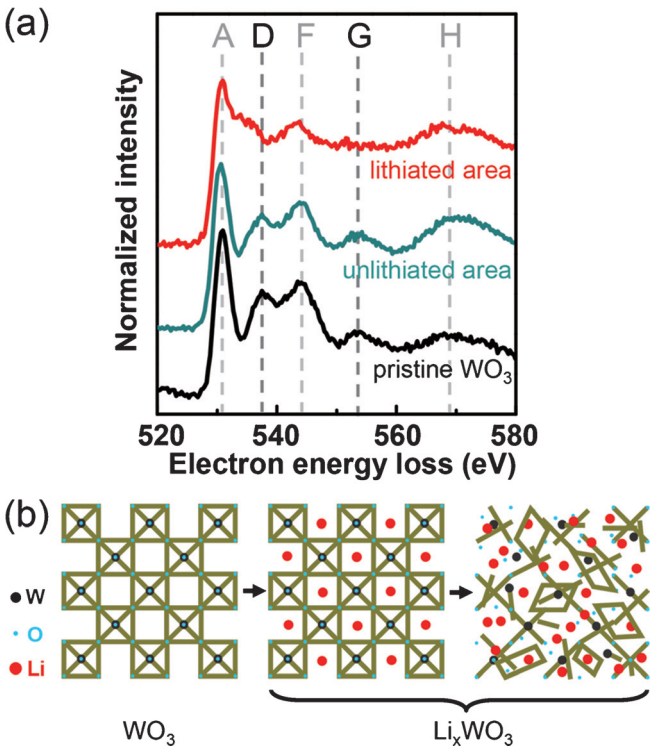

Figure 3. Revealing the structure of the product in the lithiated region by TEM-EELS investigation. a) The fine structure of the O K edge of the pristine WO_3 nanowire, the unlithiated area of the WO_3 nanowire and the deep lithiated region of the WO_3 nanowire, respectively. The number of fine structure in the EELS spetra are labeled A, D, F, G, and H. All spectra are normalized to the edge jump and vertically shifted for clarity. b) Schematic of the structural transition process from the monoclinic WO_3 phase to the amorphous Li_xWO_3 phase as a result of the deep lithiation of the WO_3 nanowire.

respectively (see the Supporting Information, Figure S2 for detailed interpretation of the spectrum). The spectrum acquired at the unlithiated area is similar to that of the pristine nanowire; however, the spectrum in the lithiated part of the wire is unlike the original one. The peak D of the lithiated area has almost disappeared. The intensity of the peak D and F is influenced strongly by the distortion of [WO_6] octahedron. The amplitude of these two peaks increases with increasing symmetry of the [WO_6] octahedron. Thus, the disappearance of peak D in the lithiated region illustrates that the [WO_6] octahedron, which is the basic unit for the monoclinic WO_3, is destroyed as a result of the lithiation reaction. Furthemore, peak G is not visible in the lithiated area, demonstrating the presence of the amorphous structure, which shows that the strong static disorder exists in the lithiated part of the nanowire.[16]

From the HRTEM, SAED, and EELS data (Figures 2, 3), it can be concluded that the near-amorphous Li_xWO_3 phase has been formed after the deep lithiation of WO_3. Then the lithiated region goes through a rapid procedure to become highly disordered. The ultimate product in the lithiated region is the compound Li_xWO_3 with an amorphous structure. In general, the WO_3 crystal, formed mainly by corner sharing of the [WO_6] octahedron, consists of lattice channels for the lithium intercalation (Figure 3b). A certain number of the lithium ions in the solid electrolyte Li_2O, and an equal amount of electrons, inject into WO_3 under the applied external electric field, thereby bringing into the lithiation effect. The lithium ions easily intercalate into the crystalline WO_3 owing to the large lattice channels. As a result, the W and O atoms break away from the crystalline WO_3, and the compound lithium tungsten bronze (Li_xWO_3) of amorphous phase then forms (Figure 3b).

It is worth noting that, apart from the Li_xWO_3, there is no reduced W as well as the segregated Li_2O, which is different from the deep lithiation process of many other metal oxides nanostuctures under in situ TEM investigation, for instance, SnO_2,[17,18] MnO_2,[19] NiO,[20] ZnO,[21] Fe_3O_4,[22] Co_3O_4,[23] CuO,[24] and RuO_2.[25] The compound Li_xWO_3, rather than the separated W and Li_2O, is generated in the deep lithiation procedure here, which is similar to that of the mild electrolyte system.[26–28] This in situ electrochemical study of the deep lithiation, in conjunction with studies of the aqueous electrolytes, completes the information of the lithiation in WO_3. These results under the extreme lithiation situation indicate that the Li_xWO_3 phase can accommodate the rapid and deep lithiation reaction well, demonstrating the high degree of chemical and structural flexibility of Li_xWO_3.

The dynamic deep lithiation process of single WO_3 nanowires is observed by the real-time BF-TEM images (Figure 4 a–f; Supporting Information, Movie S1). The interval time between two neighboring time-lapse images is 4 s. Figure 4g shows the typical corresponding L–t and I–t curves during lithiation process, of which the primary reaction occurs between 10 to 30 s. As can be seen clearly in Figure 4 b–f, the expansion, elongation and bending effects appear in the lithiated area, induced by the formation of the amorphous structure in the deep lithiated region of the nanowire. The deformation demonstrates the decreased rigidity of the

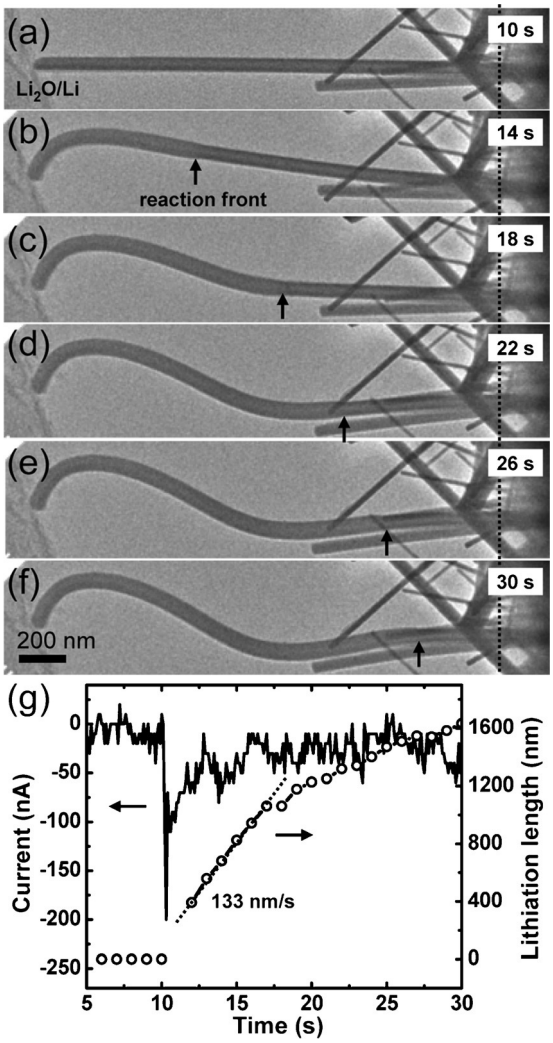

Figure 4. The dynamic deep lithiation procedure of the single WO_3 nanowire monitored in real-time (under a constant bias voltage of −2 V). a–f) Time-lapse images of the different lithiation stage in six time points. The reaction fronts are pointed out by arrows. g) The corresponding lithiation length versus time relationship (L–t curve, dotted line) and plotted current–time curve (I–t curve, dark gray line). Note that the fitted line (thin dash) shows the average lithiation velocity.

lithiated material. The lithiated length L is found to be approximately linear with respect to the reaction time ($L \propto t$) in the early stages of the lithiation procedure (Figure 4g). The average velocities of the lithiation can be estimated from the fitted L–t curve, which is 133 nm s^{-1} for 12 to 17 s. The linear relationship between the lithiation length and the reaction time indicates that the kinetics of the lithiation are likely controlled by short-ranged processes near the reaction front.[29] From 18 to 30 s, the lithiation velocity is smaller than that of 12 to 17 s, and the regular fitted curve cannot be acquired, which is due to the structural deformation of the lithiated region. The channels which the lithium ions pass through are destroyed during deep lithiation, limiting the diffusion of the lithium ions in the lithiated region. The relationship between the lithiation length and the time of the dynamic lithiation process in another WO_3 nanowire is shown

in Figure S3 (Supporting Information, Movie S2), which is similar to that of Figure 4g.

The lithiation begins between 10 and 11 s, which causes the momentary shake of the nanowire, making it difficult to determine the reaction front from the snapshot image of 10 to 11 s (Figure 4g; Supporting Information, Movie S1). Interestingly, there is an obvious current peak at 10.3 s, consistent with the beginning time point of the lithiation reaction (Figure 4g). The integration of the current peak shows that the electrons collected in the experiment is approximately 10^{12}, which is six orders of magnitude above the electrons needed during the reaction expressed by [Eq. (1)]. This analysis illustrates that the charges collected in the reaction circuit greatly exceed that of the lithiation reaction. The measurement of the current during the lithiation is believed to be important for exploring the lithiation mechanism of WO_3, which needs to be investigated further in subsequent work.

In summary, the rapid and deep lithiation of WO_3 is accomplished by driving the in situ electrochemical cell based on the WO_3 nanowire and the Li_2O solid electrolyte. The compound Li_xWO_3 of the amorphous phase is formed, without the reduced W and the segregated Li_2O phases. The movement of the lithiation reaction front interface is tracked by the real-time dynamic process. The mechanics for the lithiation of WO_3 is controlled by the short-range processes near the reaction front. The starting state of the lithiation was also investigated. These results demonstrate that the lithium tungsten bronze (Li_xWO_3) has a high degree of chemical and structural flexibility. The microstructural and dynamic evidence of the lithiation in WO_3 given by in situ TEM are crucial for the application of the WO_3-based electrochemical device.

Acknowledgements

This work was supported by the Program from Ministry of Science and Technology (Grant Nos. 2012CB933003, 2013CB932600, and 2013YQ16055107), Natural Science Foundation (Grant Nos. 11474337, 51172273, 221322304 and 11290161), and Strategic Priority Research Program B of the Chinese Academy of Sciences (Grant No. XDB07030100) of China.

Keywords: electrochemistry · in situ TEM · lithiation · phase transitions · tungsten oxide nanowires

How to cite: *Angew. Chem. Int. Ed.* **2015**, *54*, 15222–15225
Angew. Chem. **2015**, *127*, 15437–15440

[1] C.-G. Granqvist, *Nat. Mater.* **2006**, *5*, 89–90.
[2] S. K. Deb, *Sol. Energy Mater. Sol. Cells* **2008**, *92*, 245–258.
[3] C. G. Granqvist, *Thin Solid Films* **2014**, *564*, 1–38.
[4] G. A. Niklasson, C. G. Granqvist, *J. Mater. Chem.* **2007**, *17*, 127–156.
[5] H. Zheng, J. Z. Ou, M. S. Strano, R. B. Kaner, A. Mitchell, K. Kalantar-zadeh, *Adv. Funct. Mater.* **2011**, *21*, 2175–2196.
[6] B. J. Liu, J. Zheng, J. L. Wang, J. Xu, H. H. Li, S. H. Yu, *Nano Lett.* **2013**, *13*, 3589–3593.
[7] K. Bange, *Sol. Energy Mater. Sol. Cells* **1999**, *58*, 1–131.
[8] C. G. Granqvist, *Sol. Energy Mater. Sol. Cells* **2000**, *60*, 201–262.
[9] S. Yoon, C. Jo, S. Y. Noh, C. W. Lee, J. H. Song, J. Lee, *Phys. Chem. Chem. Phys.* **2011**, *13*, 11060–11066.
[10] W. Li, A. Sasaki, H. Oozu, K. Aoki, K. Kakushima, Y. Kataoka, A. Nishiyama, N. Sugii, H. Wakabayashi, K. Tsutsui, K. Natori, H. Iwai, *Microelectron. Reliab.* **2015**, *55*, 402–406.
[11] X. H. Liu, J. Y. Huang, *Energy Environ. Sci.* **2011**, *4*, 3844.
[12] C.-M. Wang, *J. Mater. Res.* **2015**, *30*, 326–339.
[13] J. Y. Huang, L. Zhong, C. M. Wang, J. P. Sullivan, W. Xu, L. Q. Zhang, S. X. Mao, N. S. Hudak, X. H. Liu, A. Subramanian, H. Fan, L. Qi, A. Kushima, J. Li, *Science* **2010**, *330*, 1515–1520.
[14] X. H. Liu, J. W. Wang, S. Huang, F. Fan, X. Huang, Y. Liu, S. Krylyuk, J. Yoo, S. A. Dayeh, A. V. Davydov, S. X. Mao, S. T. Picraux, S. Zhang, J. Li, T. Zhu, J. Y. Huang, *Nat. Nanotechnol.* **2012**, *7*, 749–756.
[15] L. Wang, Z. Xu, W. Wang, X. Bai, *J. Am. Chem. Soc.* **2014**, *136*, 6693–6697.
[16] J. Purans, A. Kuzmin, P. Parent, C. Laffon, *Electrochim. Acta* **2001**, *46*, 1973–1976.
[17] L. Zhong, X. H. Liu, G. F. Wang, S. X. Mao, J. Y. Huang, *Phys. Rev. Lett.* **2011**, *106*, 248302.
[18] C. M. Wang, W. Xu, J. Liu, J. G. Zhang, L. V. Saraf, B. W. Arey, D. Choi, Z. G. Yang, J. Xiao, S. Thevuthasan, D. R. Baer, *Nano Lett.* **2011**, *11*, 1874–1880.
[19] Y. Yuan, A. Nie, G. M. Odegard, R. Xu, D. Zhou, S. Santhanagopalan, K. He, H. Asayesh-Ardakani, D. D. Meng, R. F. Klie, C. Johnson, J. Lu, R. Shahbazian-Yassar, *Nano Lett.* **2015**, *15*, 2998–3007.
[20] K. He, H. L. Xin, K. Zhao, X. Yu, D. Nordlund, T. C. Weng, J. Li, Y. Jiang, C. A. Cadigan, R. M. Richards, M. M. Doeff, X. Q. Yang, E. A. Stach, F. Lin, D. Su, *Nano Lett.* **2015**, *15*, 1437–1444.
[21] A. Kushima, X. H. Liu, G. Zhu, Z. L. Wang, J. Y. Huang, J. Li, *Nano Lett.* **2011**, *11*, 4535–4541.
[22] Q. Su, D. Xie, J. Zhang, G. Du, B. Xu, *ACS Nano* **2013**, *7*, 9115–9121.
[23] L. Luo, J. Wu, J. Xu, V. P. Dravid, *ACS Nano* **2014**, *8*, 11560–11566.
[24] X. Wang, D. M. Tang, H. Li, W. Yi, T. Zhai, Y. Bando, D. Golberg, *Chem. Commun.* **2012**, *48*, 4812–4814.
[25] K. E. Gregorczyk, L. Yang, J. P. Sullivan, G. W. Rubloff, *ACS Nano* **2013**, *7*, 6354–6360.
[26] Q. Zhong, J. R. Dahn, K. Colbow, *Phys. Rev. B* **1992**, *46*, 2554–2560.
[27] S.-H. Lee, M. J. Seong, H. M. Cheong, E. Ozkan, E. C. Tracy, S. K. Deb, *Solid State Ionics* **2003**, *156*, 447–452.
[28] O. Pyper, A. Kaschner, C. Thomsen, *Sol. Energy Mater. Sol. Cells* **2002**, *71*, 511–522.
[29] X. H. Liu, L. Q. Zhang, L. Zhong, Y. Liu, H. Zheng, J. W. Wang, J. H. Cho, S. A. Dayeh, S. T. Picraux, J. P. Sullivan, S. X. Mao, Z. Z. Ye, J. Y. Huang, *Nano Lett.* **2011**, *11*, 2251–2258.

Received: August 30, 2015
Published online: October 16, 2015

